Neuromorphic Processing for Optical Microbead Arrays: Dimensionality Reduction and Contrast Enhancement

Baranidharan Raman, Theofilos Kotseroglou, Lori Clark, Michal Lebl, and Ricardo Gutierrez-Osuna, *Member, IEEE*

***Abstract*—This paper presents a neuromorphic approach for sensor-based machine olfaction that combines a portable chemical detection system based on microbead array technology with a biologically inspired model of signal processing in the olfactory bulb. The sensor array contains hundreds of microbeads coated with solvatochromic dyes adsorbed in, or covalently attached on, the matrix of various microspheres. When exposed to odors, each bead sensor responds with corresponding intensity changes, spectral shifts, and time-dependent variations associated with the fluorescent sensors. The bead array responses are subsequently processed using a model of olfactory circuits that capture the following two functions: chemotopic convergence of receptor neurons and center on–off surround lateral interactions. The first circuit performs dimensionality reduction, transforming the high-dimensional microbead array response into an organized spatial pattern (i.e., an odor image). The second circuit enhances the contrast of these spatial patterns, improving the separability of odors. The model is validated on an experimental dataset containing the responses of a large array of microbead sensors to five different analytes. Our results indicate that the model is able to significantly improve the separability between odor patterns, compared to that available from the raw sensor response.**

***Index Terms*—Lateral inhibition, machine olfaction, neuromorphic computation, olfactory bulb, optical microbead sensors, sensory convergence.**

I. Introduction

SENSOR-BASED instruments for odor measurement have emerged in the past two decades [1] that combine an array of cross-selective chemical sensors and a pattern recognition engine. A number of sensing technologies have been used for these instruments, primarily metal oxide and conducting polymer chemoresistors, surface acoustic wave devices, quartz microbalance resonators, and field-effect devices [2]. The vast majority of these so-called "electronic-nose" instruments employ a modest number of sensors (e.g., 4–32). In contrast, olfactory systems rely on a large number of receptor types ($\sim$1000 receptors in humans [3]), and each receptor type is massively replicated. To narrow the dimensionality gap between biological olfactory systems and their current artificial counterparts, we propose a chemical sensing approach based on optical microbead technology [4], [5]. Each microbead is a cross-selective sensor, and thousands of microbeads can be assembled into a single fiber-optic bundle. Thus, the response of a microbead array is high dimensional, combinatorial, and redundant, much like what is known about olfactory reception [6], [3].

Conventional pattern recognition techniques break down as the dimensionality of the input space grows significantly beyond the amount of training data. The olfactory system, on the other hand, has been optimized over evolutionary time to make sense of signals from millions of receptor neurons. Thus, biologically inspired computational models represent an attractive candidate for the processing of microbead array signals. Previously, Pearce *et al.* [7] investigated the role of signal integration on arrays of optical microbeads, a mechanism that also takes place in the olfactory system when receptor neurons converge onto glomeruli. The authors showed that signal integration improves the detection threshold by a factor of $\sqrt{n}$, where n is the number of beads in the array. White *et al.* [8], [9] employed a spiking neuron model of the peripheral olfactory system to process signals from fiber-optic sensor array. In their model, the response of each sensor was converted into a pattern of spikes across a population of olfactory receptor neurons (ORNs), which then projects to a unique mitral cell. Different odors produce unique spatio-temporal activation patterns across mitral cells, which are then discriminated with a delay-line neural network (DLNN). Their olfactory bulb-DLNN model is able to produce a decoupled odor code: odor quality being encoded by the spatial activity across units, and odor intensity by the response latency of the units.

In this paper, we extend a biologically inspired model that we proposed for temperature-modulated metal–oxide sensors [10]. The model captures the following two stages in the olfactory pathway: chemotopic convergence of receptor neurons

Manuscript received May 24, 2006; revised October 12, 2006; accepted October 13, 2006. The Illumina team was supported by Chevron Texaco. The work of B. Raman and R. Gutierrez-Osuna was supported by the National Science Foundation under CAREER award 9984426/0229598. The associate editor coordinating the review of this manuscript and approving it for publication was Prof. Fabian Josse.

B. Raman was with the Computer Science Department, Texas A&M University, College Station, TX 77843 USA. He is now with the Process Sensing Group, the National Institute of Standards and Technology, Gaithersburg, MD 20899-8362 USA (e-mail: braman@nist.gov).

T. Kotseroglou was with Illumina, Inc., San Diego, CA 92121 USA. He is now with ORAMIC LLC, San Carlos, CA 94070 USA (e-mail: theo@selvamedical.com).

L. Clark and M. Lebl are with Illumina, Inc., San Diego, CA 92121 USA (e-mail: loriclark@suscom-maine.net; mlebl@illumina.com).

R. Gutierrez-Osuna is with the Computer Science Department, Texas A&M University, College Station, TX 77843 USA (e-mail: rgutier@cs.tamu.edu).

Color versions of one or more of the figures in this paper are available online at http://ieeexplore.ieee.org.

Digital Object Identifier 10.1109/JSEN.2007.891935

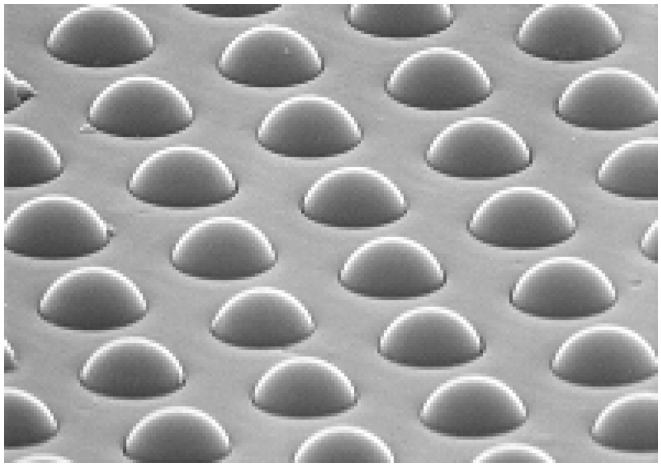

Fig. 1. Scanning electron microscope (SEM) image of a microbead array (Illumina's BeadArray™). Each bead has a diameter of 3 μm, and protrudes out of a well of similar diameter etched onto a fiber-optic bundle.

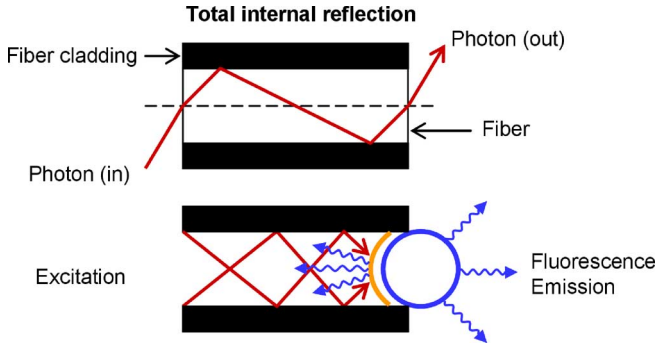

Fig. 2. The optical fiber property of total internal reflection is used to guide excitation light, generated at the proximal end of the fiber, towards a bead at the distal end of the fiber. The dye on the bead is excited, and the generated fluorescence is guided back towards the proximal end in order to be analyzed.

onto the olfactory bulb and center on–off surround lateral interactions. The first circuit performs dimensionality reduction, transforming the high-dimensional response into an organized spatial pattern (i.e., an odor image). The second circuit reduces the overlap between these patterns, increasing their discrimination at a later stage. The model is validated on an experimental dataset containing the responses of a large array of microbead sensors ($N = 586$ sensors) to five different analytes.

II. Optical Microbead Sensor Arrays

The microbead array technology used in this research was originally developed by Walt and colleagues at Tufts University [4], [5]. Typically, each array includes thousands of bead sensors that are made from various materials (e.g., Si or PMMA) that can be porous in order to increase surface areas. Beads are arranged in wells etched on the solid surface in order to generate an array of sensors, as illustrated in Fig. 1.

The beads are functionalized using solvatochromic dyes, either adsorbed in the matrix of the microspheres, or covalently attached to them. Solvatochromic dyes are known to display large shifts in their fluorescence spectra with variations in the polarity of the surrounding medium, a property that is retained even after the dyes are applied to the beads. Unique sensors can be made either by immobilizing the solvatochromic dyes in polymer matrices that vary in polarity, hydro-phobicity, porosity, elasticity, and swelling tendency, or by using different dyes with the same matrix. In this study, the former approach was used.

The size of each sensor is in the order of a few micrometers (3–5 μm in this study), so one can easily envision a miniaturized multisensor system. Illumina's BeadArrayTM technology allows us to build arrays that contain 50 000 or more fibers, with micron-size cores in a 1.5-mm-diameter fiber bundle. The cores of the fibers are etched on one side of the fiber bundle using a chemical method to a specific depth, while the cladding of each fiber remains intact. This means that there exist 50 000 microwells at one end of the fiber bundle, which can be randomly loaded with the functionalized microspheres. Light excitation and fluorescence collection from the fiber bundle is achieved in a variety of ways; an example is illustrated in Fig. 2.

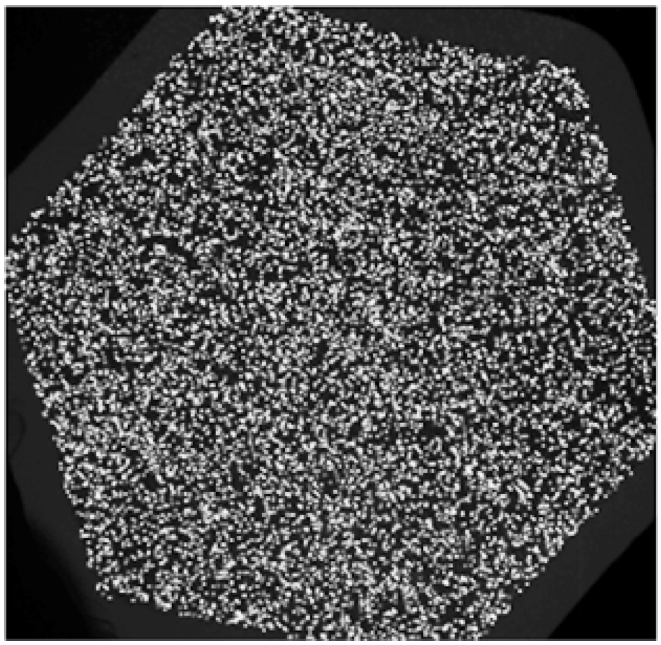

Fig. 3. Image of a monochrome CCD camera of the fluorescence pattern of an array. The image was filtered using a bandpass optical filter matched to the maximum response of the solvatochromic dye.

Different methods have been employed for fluorescence detection, such as a spatially distributed readout with a broadband light excitation source, an integrated spectrometer detector, and a hyperspectral imaging technique whereby spatially distributed signals are collected via a fast-changing electronically tunable optical filter. In the latter case, a snapshot of the spectra of each individual sensor in the array is recorded at each instant in time. In this study, the detector is a charge-coupled device (CCD) camera that can record (in a single image) the fluorescence pattern of all beads, filtered with a specific bandwidth optical filter that matches the maximum response of the solvatochromic dye used in the sensors. Fig. 3 shows an example fluorescence pattern of a microbead array recorded using a monochrome CCD camera. The selection methodology used to determine an appropriate bandpass filter is illustrated in Fig. 4.

The distribution of bead types in the fiber bundle is random, as shown in Fig. 5. Hence, each array first needs to be decoded to identify the position and type of each bead in the image. This is

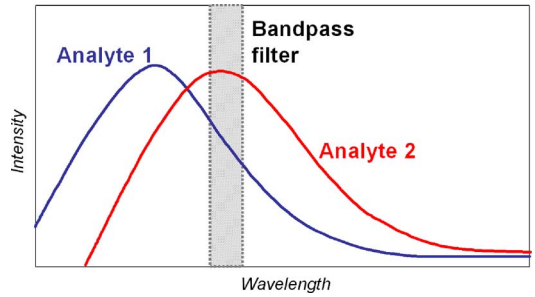

Fig. 4. Detection principle: the wavelength shift is captured as an intensity change with an optical bandpass filter appropriately designed for the specific emission fluorescence.

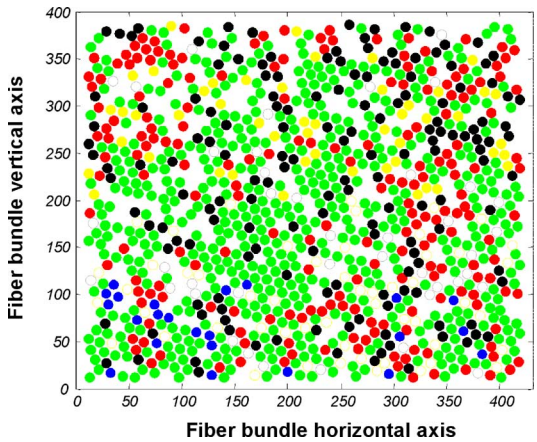

Fig. 5. Random distribution of five bead sensors across the fiber bundle (each color represents a specific bead sensor).

accomplished by exposing the array to a number of known solvent vapors, to which the individual bead types have been previously calibrated [11]. After decoding, one can then analyze in various ways a series of such images collected over the duration of the sensor–sample interaction. Analysis of the intensity variations at a particular fluorescence wavelength during an image sequence generates a unique temporal response pattern for each bead type, creating a "fingerprint" for each chemical sample. Subsequent pattern recognition of the bead array responses allows identification of the chemical.

III. Experimental Setup

Experimental data for this work was collected from a benchtop system used at Illumina to screen single sensors (specificity and sensitivity), analyze multisensor array data at the interaction of various chemicals, perform spectral studies, and optimize image acquisition. A first-generation compact system has also been developed and tested specifically for the petroleum industry (ChevronTexaco). This portable device is shown in Fig. 6. Various designs of a miniature detector have also been explored that could be integrated with a wireless network infrastructure for distributed sensing applications.

A. The Optical Module

A block diagram of the optical module in the benchtop system is shown in Fig. 7. The excitation light is generated by a white

Fig. 6. Portable, field deployable chemical sensing unit.

light source, and filtered by a combination of interference bandpass optical filters to allow only an optimized excitation spectrum to reach the sensor. The excitation light is directed in a typical epi-fluorescence setup, whereby a beamsplitter is used to both excite the sensor and also select the emitted fluorescence from the sensor in a straight path to the CCD. The CCD is a cooled VGA camera (Cooke Corporation) with 6×6 μm pixel size and very high quantum efficiency (QE) in the wavelengths necessary for an optimum spectral shift. A $20\times$ scientific grade objective (Olympus U-PLAN APO), optimized for all wavelengths, is used to image the fiber-optic bundle. The sensor is a fiber-optic bundle etched and fitted with approximately 50 000 bead sensors. However, the field of view of the objective spans only a quarter of the full fiber-bundle surface, so a reduced number of sensors in the array can be imaged at any point in time.

The interaction chamber was made out of Teflon (and/or PEEK, depending on the chemicals tested), and was designed with a goal of ultra-low dead volume. The sensor was fitted via a leak-tight ferrule onto the threads of one of the ports of the chamber; two additional ports were used for delivery and exhaust. A fourth port, not used in this experiment, can also be used for head-on excitation. In this alternative setup, fluorescence is collected through the bundle rather than through epi-fluorescence, making it advantageous for a compact device with light-emitting diode (LED) illumination sources.

B. Vapor-Delivery Module

The vapor-delivery module consists of latching solenoid valves, a micro-pump, and the interaction chamber that houses the sensor. Teflon tubing, as well as appropriate sample and purge gas (air) filters, are used. The delivery system can be alternated between liquid and gas phases. Two configurations are available in the gas phase: a calibration mode, where a system of syringes and solenoids and/or sampling bags is used, and a detection mode. The syringe/solenoid configuration is described in Fig. 8. N_2 is sparged through the sample, so that vapor builds up in the headspace of the bottle until equilibrium is reached. A solenoid valve (V1) oscillates between headspace (V1 closed) and the N_2 gas (V1 open), while the syringe is

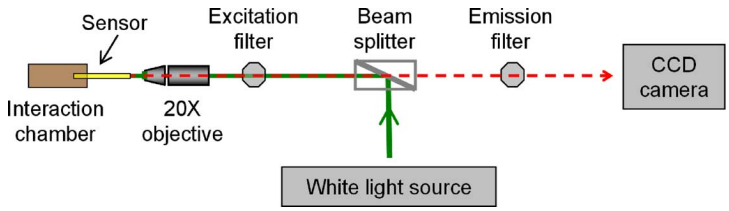

Fig. 7. The optical module of the Illumina benchtop system.

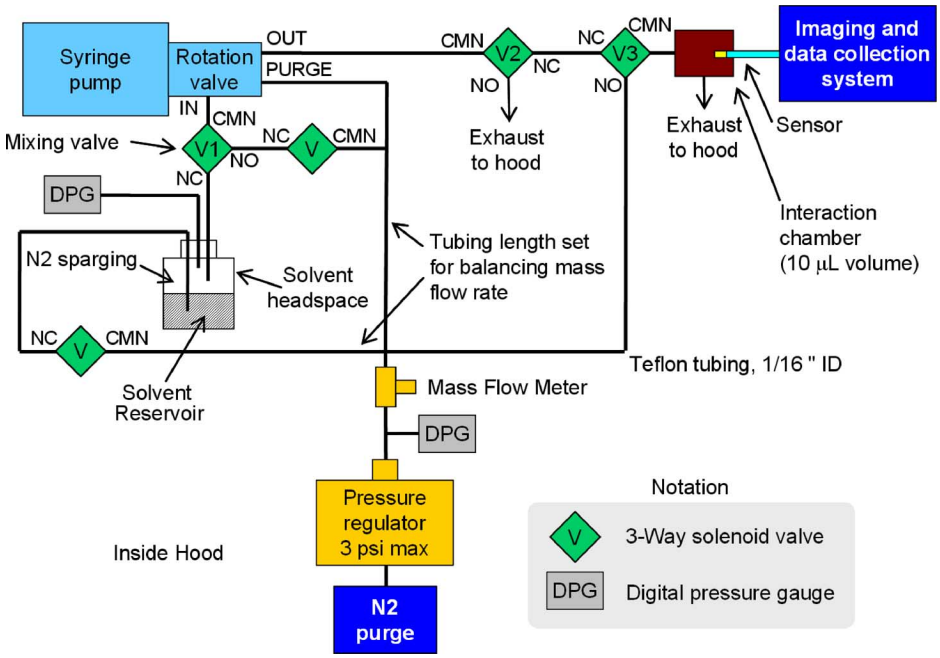

Fig. 8. Sample delivery system used for calibration of the portable device.

aspirating to capture this mixture. Then the syringe dispenses, creating a constant flow and concentration of the sample in the carrier gas stream, and is continuously released in the hood when the top left solenoid valve (V2) is at the normally-open (NO) position. At the same time, the sensor is purged with N2 by keeping the right solenoid (V3) at NO position. Following purging, both V2 and V3 are set to a closed position, allowing the diluted sample to flow onto the sensor for a specified amount of time (of the order of 1 to 6 s). Finally, the system returns back to the N_2 purging initial condition (V2 and V3 at NO position).

The system was calibrated using low flow techniques and Tedlar bags at very high dilution numbers. The resolution of the system (i.e., minimum detectable difference in concentration) is of the order of 1 to 5 ppm, depending on the solvent vapor. The sensors with highest specificity (optimized) display a limit of detection (LOD) in the order of 10 to 50 ppm, depending on the solvent vapor tested, under laboratory conditions.

C. Control Electronics and Data Acquisition

Currently, a laptop computer controls all the electronics of the optical system, as well as the vapor delivery system, and the data acquisition. Details of this system are to be published as a separate paper in the near future.

D. Experimental Dataset

The experimental dataset used in this study comprises of transient responses of 586 microbead sensors to five analytes: toluene (TOL), ethyl alcohol (EA), acetone (ACE), ethyl hydroxide (Et-OH), and methyl hydroxide (Me-OH). Fig. 9(a) shows the transient response of 100 microbead sensors to acetone, whereas Fig. 9(b) shows the transient response of a single microbead sensor to several presentations of each analyte. The odorant was introduced at $t = 14$ s and removed at $t = 35$ s.

IV. Computational Modeling

The use of large arrays (hundreds to thousands of sensors) opens the doors for alternative pattern recognition approaches. The approach adopted in this study involves mimicking solutions from the biological olfactory system [15]. Specifically, we model two computational functions in the olfactory pathway: chemotopic convergence and odor opponency, for processing bead array responses. Details of these models are presented in the following subsections.

A. Dimensionality Reduction Through Chemotopic Convergence

The projection from the olfactory epithelium onto the olfactory bulb is organized such that ORNs expressing the same receptor gene converge onto one or a few spherical structures

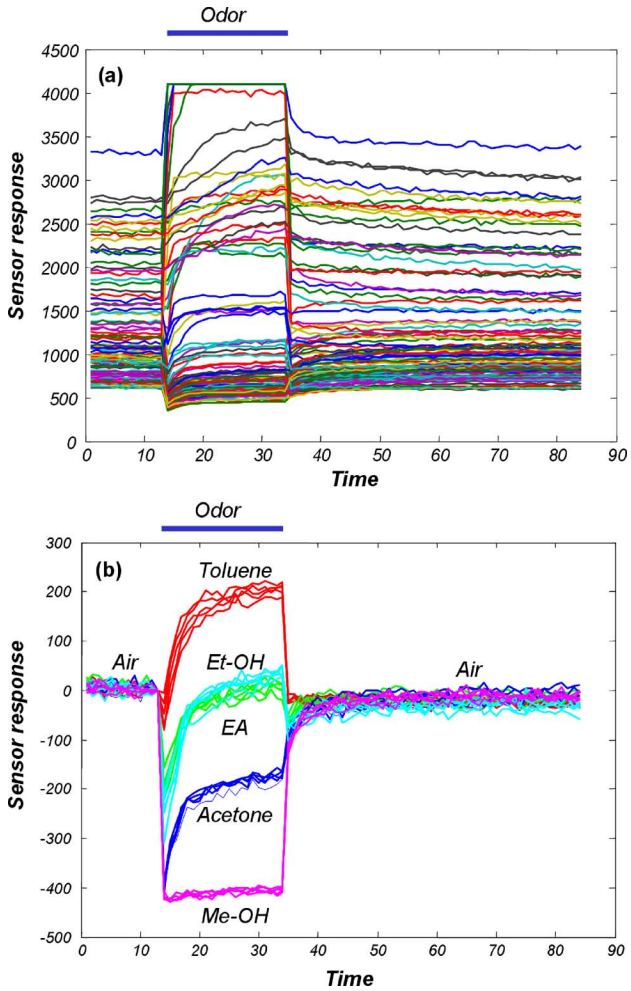

Fig. 9. (a) Response of 100 microbead sensors to acetone. The odor is introduced at $t = 14$ s and removed at $t = 35$ s. (b) Transient response of a single microbead sensor to several presentations of each analyte.

of neuropil called glomeruli, where they synapse mitral cell dendrites [16]. This convergence transforms the initial combinatorial code into an organized spatial pattern (i.e., an olfactory image), which decouples odor identity from intensity [17]. In addition, massive convergence improves the signal-to-noise ratio by integrating signals from multiple receptor neurons [7], [18].

To model the ORN-glomerular convergence, we topologically cluster sensors that have similar selectivity using the self-organizing map (SOM) of Kohonen [19]. The selectivity of a bead sensor is defined as

$$Sel_i = \left[R_i^{O_1}, R_i^{O_2}, \ldots, R_i^{O_C}\right] \tag{1}$$

where R_i^O is the response of sensor i to odor O, and C is the number of odorants. Once the SOM is trained, the response of each SOM node can be computed as follows:

$$G_j^O = \frac{\sum_{i=1}^{N} W_{ij} R_i^O}{\sum_{i=1}^{N} W_{ij}} \tag{2}$$

where N is the number of bead sensors, and $W_{ij} = 1$ if sensor i converges to SOM node j and zero otherwise; a normalization constant $\sum_{i=1}^{N} W_{ij}$ is used to ensure that discriminatory information is not overshadowed by the common-mode response of the array [10]. Note that the SOM is used to cluster features (bead sensors) rather than samples (as is conventionally done in pattern recognition). Thus, each SOM node G_j can be thought of as a simulated glomerular unit.

B. Contrast Enhancement Through Center On–Off Surround Lateral Interaction

The initial odor image available at the glomerular layer is further transformed in the olfactory bulb (OB) by means of two distinct lateral inhibitory circuits. The first of these circuits, which occurs at the input of the OB, has been suggested to perform some form of "volume control" to broaden the dynamic range of concentrations at which an odorant can be identified [20]. A computational model of this circuit has been previously described by us to achieve concentration normalization [21]. The second circuit occurs at the output of the OB. These circuits have been recently found to have local excitatory (on-center) and long-range inhibitory (off-surround) connections, and have been suggested to perform contrast enhancement of the spatial patterns in the OB [22].

We model this center on–off surround contrast-enhancement circuit with the well-established additive model from neurodynamics [23, p. 676], whose general form is

$$\frac{dv_j(t)}{dt} = -\frac{v_j(t)}{\tau_j} + \sum_{k=1}^{M} L_{kj}\varphi\left(v_k(t)\right) + I_j \tag{3}$$

where v_j is the activity of mitral neuron j, τ_j is the time constant that captures the dynamics of the neuron, L_{kj} is the synaptic weight between neurons k and j, M is the number of neurons, and I_j is the external input in (2), properly scaled ($I_j = 10G_j$) in order to balance the contribution of sensors and lateral inputs. The nonlinear activation $\varphi(\cdot)$ is the logistic function defined by

$$\varphi(v_j) = \frac{1}{1 + \exp(-a_1 \cdot (v_j - a_2))} \tag{4}$$

where the constants a_1 and a_2 are set to 0.0392 and 74.985, respectively, to match the dynamic range of the input signal from microbead arrays.[1] To model center on–off surround, each neuron makes excitatory synapses to nearby units and inhibitory synapses with distant units as follows:

$$L_{kj} = \begin{cases} U[a,b], & d(k,j) \le \frac{\sqrt{M}}{r} \\ U[-b,a], & \frac{\sqrt{M}}{r} < d(k,j) < \frac{2\sqrt{M}}{r} \\ 0, & d(k,j) \ge \frac{2\sqrt{M}}{r} \end{cases} \tag{5}$$

where $U[a,b]$ is a uniform distribution between a and b ($a = 0$, $b = 1$ in this study), d is the distance between units measured as a Euclidean distance within the lattice

[1]The value of these constants is problem dependent, but can be easily tuned so that most units in the lattice operate in the near-linear range of the sigmoidal function; this ensures good sensitivity to changes in the sensor response. An inappropriate choice for these values would otherwise lead to saturation of these units.

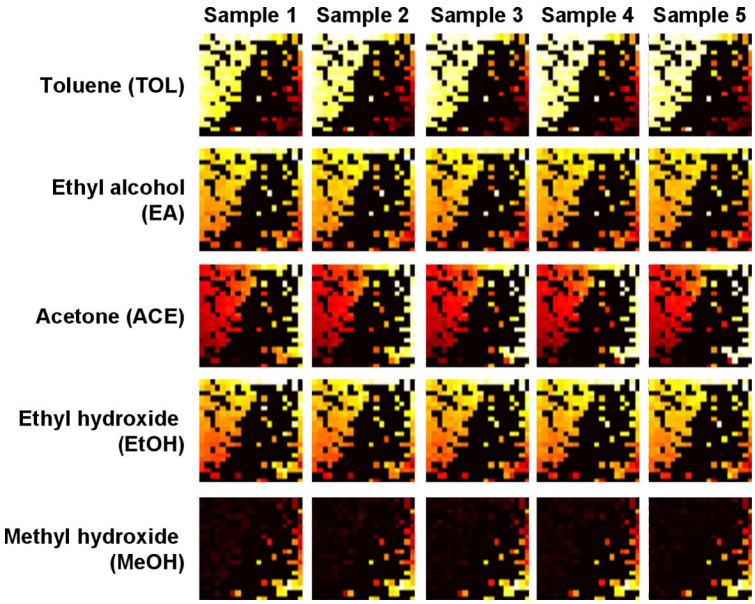

Fig. 10. Simulated glomerular maps for five analytes, five repetitions each, using a 20×20 SOM lattice and 586 microbead sensors.

($d = \sqrt{(row_k - row_j)^2 + (col_k - col_j)^2}$; *row* and *col* being the row and column coordinates of a neuron in the lattice), and r determines the receptive-field width of the lateral connections. An appropriate lateral inhibition spread (r) is selected to provide maximum odor separability, where separability is measured as follows [24]:

$$J = \frac{tr(S_B)}{tr(S_W)} \tag{6}$$

where S_W and S_B are the within-class and between-class scatter matrices, respectively [25]. For the dataset presented in Section III-D, the maximum for this separability measure was found to occur at $r = 4.3$ (cells or pixels). This receptive field width will be used to quantify the benefits of the proposed model.

V. Results

We used the response of 586 microbeads to the five analytes (Section III-D) to train a chemotopic convergence map with 400 nodes, arranged as a 20×20 lattice. The response of each sensor to an odorant was the difference between the steady-state response ($t = 34$ s and baseline value ($t = 13$ s). Fig. 10 shows the resulting odor maps for the five analytes, five samples per analyte. Only the first sample of each odor was used to train the SOM; all remaining samples were used for validation purposes. It can be observed that each analyte is encoded by a unique spatial pattern across the SOM lattice, and that these patterns are highly repeatable across presentations.

The outputs of the convergence model were subsequently input to the additive lateral inhibition model in (3). Fig. 11 (top row) shows the spatial patterns that result from sensory convergence at the input of the OB for one validation sample of each analyte (i.e., Fig. 10, first column). These spatial patterns are highly overlapping due to the collinearity of the sensors. Fig. 11 (middle row) shows the resulting spatial activities following stabilization of the center-surround lateral interactions.

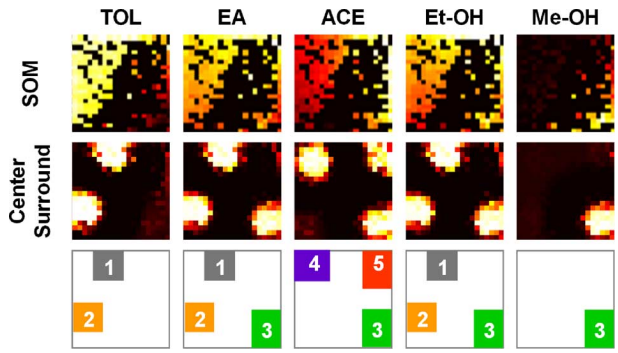

Fig. 11. Spatial maps at the input (top row) and output (middle row) of the OB model. The bottom row shows the four sparse coding regions that emerge as a result of the lateral interactions.

TOL leads to heavy activation on two highly localized regions (spatial code: 12). EA and Et-OH, which generate similar sensor response, produce similar activation in regions 1, 2, and 3 (spatial code: 123). ACE produces heavy activation of region 4, 5, and 3 (spatial code: 345). Finally, Me-OH produces heavy activation of regions 3 alone (spatial code: 3). Thus, the spatial patterns after center-surround interactions are significantly sparser than the chemotopic odor maps, and provide increased odor separability.

The spatial patterns in Fig. 11 capture information that is available from the steady-state response of the model. However, a growing body of evidence indicates that time and dynamics are key to odor information processing [18], [26]. To visualize their role in the behavior of our model, the temporal evolution of the 400-dimensional (20×20) system was projected onto a three-dimensional subspace by means of principal components analysis. Shown in Fig. 12, trajectories for each odor originate at nearby locations in state space; this initial state corresponds to the highly overlapping spatial patterns at the input of OB (i.e., those in Fig. 11, top row). As a result

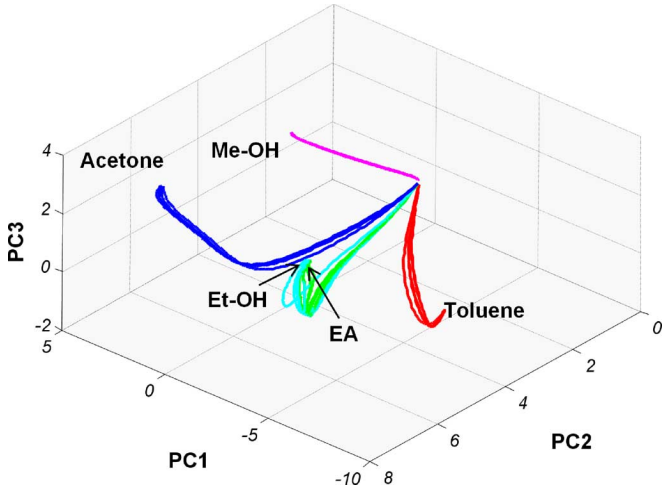

Fig. 12. Evolution of OB activity for the five analytes along the first three principal components. Twenty-five trajectories are shown, one per sample in the dataset. The initial points in the trajectories are the spatial maps at the input of the OB network, shown in Fig. 11 (top row). Odor separability is significantly improved as a result of lateral inhibition.

of center on–off-surround lateral connections, the activity for each odor slowly moves away from the initial location and settles into odor-specific fixed-point attractors, which correspond to the localized spatial patterns in Fig. 11 (middle row). The repeatability of the odor trajectories is illustrated by visualizing all twenty-five trajectories (five samples per analyte) in the dataset. These results are consistent with recent neurobiological findings in the insect antennal lobe (analogous to mammalian olfactory bulb), which show that odor-evoked spatiotemporal activity evolves over time and converges into odor-specific attractors [26].

Visual inspection of the steady-state response in Fig. 11 and the transient trajectories in Fig. 12 clearly shows that the lateral inhibitory network increases the contrast between odors. To quantify these benefits, we compared the separability measure J in (6) at the output of the model against the separability that is available 1) from raw sensor data, 2) following chemotopic convergence, and 3) at the output of an OB network with random lateral connections. The latter allows us to separate the role of center on–off surround circuits from that of dynamics alone. Fig. 13 shows the temporal evolution of the separability J for each of the four cases. Three repetitions are shown in the case of random and center-surround lateral connections to illustrate the repeatability of results for different (randomly drawn) connection strengths. Chemotopic convergence alone ($J = 83$) is able to improve odor separability compared to that available from the raw bead-array response ($J = 60$). Random lateral connections appear to improve discrimination initially ($J \sim 500$ at $t = 50$ ms), but their steady-state performance is on average comparable to chemotopic convergence. In contrast, discrimination for the model with center on–off surround lateral connection increases monotonically after an initial period ($t >$ 100 ms), reaching a maximum in their steady-state response ($J \sim 700$). This steady-state discrimination corresponds to the fixed-point attractors in Fig. 12 and the spatial maps in Fig. 11 (middle row).

A. Comparison With Statistical Techniques

We compared the pattern separability achieved by the proposed model against two statistical dimensionality-reduction techniques that are widely used with chemical sensor array data: principal component analysis (PCA) and linear discriminant analysis (LDA) [25]. PCA is an unsupervised method that provides optimum reconstruction in the mean-squared-error sense, whereas LDA is a supervised technique that provides optimum separability for Gaussian classes with equal covariance matrices.

PCA was performed on the raw sensor data (586 dimensions). Only the first two PCA eigenvectors were preserved, which account for 96.2% of the variance. LDA was also performed on the raw sensor data; in this case, the four nonzero eigenvalues were preserved. Both statistical techniques provide good separation between odor classes, but lead to larger within-class scatter than the neuromorphic approach; e.g., note in Fig. 12 that the network converges to a highly localized activity pattern when exposed to multiple repetitions of the same odor. As a result, the neuromorphic model provides higher odor separability (J) than PCA and LDA, as illustrated in Fig. 13. While the extent to which these results generalize to other datasets requires further investigation, we believe that the improved performance of the neuromorphic model is due to the fact that it does not require computation of inverse scatter matrices, which become problematic when the dimensionality of the input space is larger than the number of samples in the dataset (e.g., 586 dimensions versus five samples per class, in our case). This suggests that the neuromorphic model is particularly advantageous in very-high-dimensional spaces, a result that is consistent with the olfactory system.

VI. Summary

In this paper, we have presented a neuromorphic approach for sensor-based machine olfaction that combines microbead array technology with a model of signal processing in the olfactory bulb. Our approach can be summarized as follows. Polymeric microbeads with immobilized solvatochromic dyes are randomly assembled in a fiber bundle to produce an array of diverse sensors. Changes in polarity of the dyes' local environment induce characteristic shifts in their fluorescence spectrum, which can be monitored. Imaging of the microbeads' response leads to a high-dimensional signal, which is first processed with a self-organizing model of chemotopic convergence. The convergence model transforms the microbead array response into an organized spatial pattern (i.e., an odor image). Odor images formed through convergence are however highly overlapping due to collinearity of sensor input, and require further processing. Hence, these odor maps are subsequently processed using a lateral inhibitory circuit with center-surround connections. These lateral interactions improve contrast between odor images, producing sparse and more orthogonal patterns than those available at the input.

At present, the steady-state response of the bead sensors to odorants is used as the input to our model. We are currently investigating the extent to which information in the response transients can further improve separability between similar odors (e.g., EA versus Et-OH). Specifically, one could modulate the

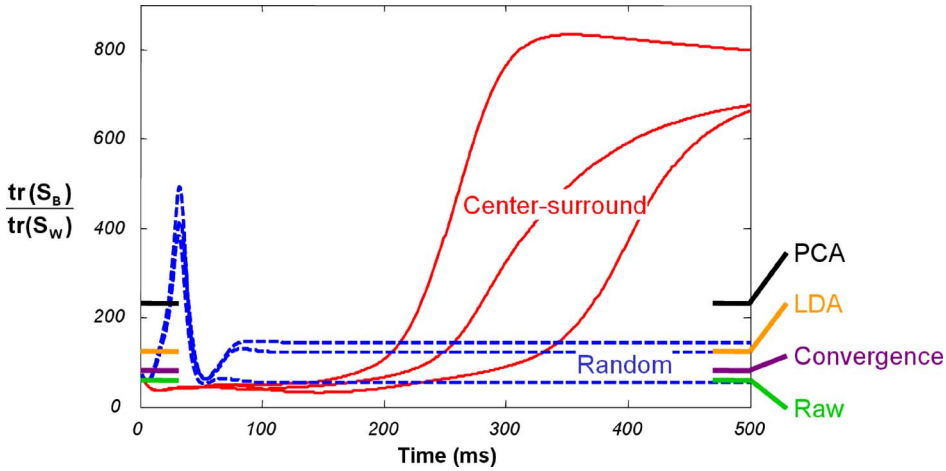

Fig. 13. Comparison of the OB network with center-surround lateral connections (three repetitions are shown) against 1) raw data, 2) following chemotopic convergence, 3) at the output of an OB with random lateral connections (three repetitions), 4) PCA (first two components capturing 96.15% of total variance), and, 5) LDA.

sensors with a pulse train in the sample concentration, much like what is observed with the breathing cycle of animals. This would lead to oscillatory attractors in the model. By matching the time constants of the model to those of the sensor transients, the system could converge to limit cycles with higher discriminatory information than the fixed-point attractors in Fig. 12. Further, this work has focused on primarily discriminating pure analytes at a single concentration. The next stage of our research will investigate incorporation of gain-control circuits in the olfactory bulb to handle multiple concentrations [27], and bulb–cortex interaction to perform mixture segmentation and background suppression [28].

ACKNOWLEDGMENT

The authors wish to thank Dr. D. Young of ChevronTexaco for his support of the Optical Nose Project.

REFERENCES

[1] K. C. Persaud and G. H. Dodd, "Analysis of discrimination mechanisms of the mammalian olfactory system using a model nose," *Nature*, vol. 299, pp. 352–355, 1982.

[2] H. T. Nagle, S. S. Schiffman, and R. Gutierrez-Osuna, "The how and why of electronic noses," *IEEE Spectrum*, vol. 35, no. 9, pp. 22–34, 1998.

[3] R. Axel, "The molecular logic of smell," *Scient. Amer.*, vol. 273, no. 4, pp. 154–159, 1995.

[4] T. A. Dickinson, J. White, J. S. Kauer, and D. R. Walt, "A chemical detecting system based on cross-reactive optical sensor array," *Nature*, vol. 382, no. 22, pp. 697–700, 1996.

[5] T. A. Dickinson, K. L. Michael, J. S. Kauer, and D. R. Walt, "Convergent, self-encoded bead sensor array in the design of an artificial nose," *Anal. Chem.*, vol. 71, pp. 2192–2198, 1999.

[6] G. Sicard and A. Holley, "Receptor cell responses to odorants: Similarities and differences among odorants," *Brain Res.*, vol. 292, pp. 283–296, 1984.

[7] T. C. Pearce, P. F. M. J. Verschure, J. White, and J. S. Kauer, "Robust stimulus encoding in olfactory processing: Hyperacuity and efficient signal transmission," in *Emergent Neural Computation Architectures Based on Neuroscience*, S. Wermter, J. Austin, and D. Willshaw, Eds. New York: Springer-Verlag, 2001, pp. 461–479.

[8] J. White, T. A. Dickinson, D. R. Walt, and J. S. Kauer, "An olfactory neural network for vapor recognition in an artificial nose," *Biol. Cybern.*, vol. 78, pp. 245–251, 1998.

[9] J. White and J. S. Kauer, "Odor recognition in an artificial nose by spatio-temporal processing using an olfactory neuronal network," *Neurocomputing*, vol. 26–27, pp. 919–924, 1999.

[10] B. Raman, R. Gutierrez-Osuna, A. Gutierrez-Galvez, and A. Perera-Lluna, "Sensor-based machine olfaction with a neurodynamics model of the olfactory bulb," in *Proc. 2004 IEEE/RSJ Int. Conf. Intelligent Robots and Systems*, Sendai, Japan, 2004, vol. 1, pp. 319–324.

[11] K. J. Albert, D. S. Gill, T. C. Pearce, and D. R. Walt, "Automatic decoding of sensor types within randomly-ordered, high-density optical sensor arrays," *Anal. Bioanal. Chem.*, vol. 303, no. 8, pp. 792–802, 2002.

[12] U. Weimar and W. Gopel, "Chemical imaging: Trends in multiparameter sensor system," in *Proc. Workshop on Intelligent Sensors*, Aachen, Germany, 1999.

[13] A. P. Lee and B. J. Reedy, "Temperature modulation in semiconductor gas sensing," *Sens. Actuat.*, vol. B60, pp. 35–42, 1999.

[14] R. Gutierrez-Osuna, A. Gutierrez-Galvez, and N. Powar, "Transient response analysis for temperature-modulated chemoresistors," *Sens. Actuat. B*, vol. 93, pp. 52–66, 2003.

[15] B. Raman, P. Sun, A. Gutierrez-Galvez, and R. Gutierrez-Osuna, "Processing of chemical sensor arrays with a biologically-inspired model of olfactory coding," *IEEE Trans. Neural Netw.*, vol. 17, no. 4, pp. 1015–1024, Jul. 2006.

[16] R. Vassar *et al.*, "Topographic organization of sensory projections to the olfactory bulb," *Cell*, vol. 79, pp. 981–991, 1994.

[17] R. Gutierrez-Osuna, "A self-organizing model of chemotopic convergence for olfactory coding," in *Proc. Joint EMBS-BMES Conf.*, Houston, TX, 2002, pp. 23–26.

[18] G. Laurent, "A systems perspective on early olfactory coding," *Science*, vol. 286, pp. 723–728, 1999.

[19] T. Kohonen, "Self-organized formation of topologically correct feature maps," *Biol. Cybern.*, vol. 43, pp. 59–69, 1982.

[20] W. Freeman, "Olfactory system: Odorant detection and classification," in *Building Blocks for Intelligent Systems: Brain Components as Elements of Intelligent Function*, D. Amit and G.Parisi, Eds. San Diego: Academic, 1999, vol. III, pt. 2.

[21] B. Raman and R. Gutierrez-Osuna, "Concentration normalization with a model of gain control in the olfactory bulb," *Sens. Actuat.*, vol. B 116, no. 1–2, pp. 36–42, Jul. 2006.

[22] J. L. Aungst, P. M. Heyward, A. C. Puche, S. V. Karnup, A. Hayar, G. Szabo, and M. T. Shipley, "Center-surround inhibition among olfactory bulb glomeruli," *Nature*, vol. 26, pp. 623–629, 2003.

[23] S. Haykin, *Neural Networks: A Comprehensive Foundation*, 2nd ed. Englewood Cliffs, NJ: Prentice-Hall, 1999, p. 676.

[24] K. Fukanaga, *Statistical Pattern Recognition*, 2nd ed. San Diego, CA: Academic Pr., 1990.

[25] R. O. Duda, P. E. Hart, and D. G. Stork, *Pattern Classifacation*, 2nd ed. New York: Wiley-Interscience, 2000.

[26] R. F. Galán, S. Sachse, C. G. Galizia, and A. V. Herz, "Odor-driven attractor dynamics in the antennal lobe allow for simple and rapid olfactory pattern classification," *Neural Comput.*, vol. 16, no. 5, pp. 999–1012, 2003.

[27] B. Raman and R. Gutierrez-Osuna, "Concentration normalization with a model of gain control in the olfactory bulb," in *Proc. 11th Int. Symp. Olfaction and the Electronic Nose (ISOEN 2005)*, Barcelona, Spain, Apr. 13–15, 2005.

[28] ——, "Mixture segmentation and background suppression in chemosensor arrays with a model of olfactory bulb-cortex interaction," in *Proc. 2005 IEEE Inte. Joint Conf. Neural Networks*, Montreal, QC, Canada, Jul.-Aug. 31–4, 2005, vol. 1, pp. 131–136.

Baranidharan Raman received the B.S. degree in computer science with distinction from the University of Madras, Madras, India, in 2000 and the M.S. and Ph.D. degrees in computer science from Texas A&M University, College Station, in 2003 and 2005, respectively.

He is currently an NIH/NIST joint Postdoctoral Fellow in the Laboratory of Cellular and Synaptic Neurophysiology (NICHD), and the Process Sensing Group (NIST), National Institute of Standards and Technology, Gaithersburg, MD. His research interests include combining computational and electrophysiological approaches to study neural computations especially olfactory signal processing, sensor-based machine olfaction, machine learning, intelligent systems and robotics, human–computer interaction, and dynamical systems.

Theofilos Kotseroglou received the B.S. degree in physics from the University of Athens, Athens, Greece in 1990 and the Ph.D. degree in physics from the University of Rochester, Rochester, NY, in 1996.

From 1996 to 2000, he was engineering physicist at the Stanford Linear Accelerator Center, Stanford University, Stanford, CA. He subsequently joined Illumina's Engineering Department, San Diego, CA, initially to develop a chemical detection system based on bead array technology. In 2005, he co-founded and was Senior Vice-President, Research and Development, of Selva Medical Inc., developing a laser–catheter device for the treatment of stroke. Selva Medical was acquired by the medical division of W. L. Gore & Associates in 2006. He is currently General Partner at Oramic LLC., San Carlos, CA. His research interests include lasers and photonics, especially in applications of biotechnology, chemical detection, and medical devices.

Lori Clark received the B.S. degree in chemistry in 1993 from Old Dominion University, Norfolk, VA. She continued her education at Old Dominion University as a NASA Graduate Research Fellow and received the M.S. degree in analytical chemistry in 1996.

From 1996 to 1999, she worked for Sulzer Carbomedics, a manufacturer of mechanical heart valves. She joined Illumina, Inc., San Diego, CA as a Research Associate in January 2000.

Michal Lebl graduated from The University of Chemical Technology (VSCHT) in Prague, Czechoslovakia, in 1974. He finished his Ph.D. studies at the Institute of Organic Chemistry and Biochemistry of the Czechoslovak Academy of Sciences, Prague, in 1978. In 1992, he defended his D.Sc. (organic chemistry) title in the same institution.

In 1991, he moved to the United States and worked as the Director of Chemistry in Selectide Corporation, the first combinatorial chemistry company in the world, in Tucson, AZ. In 1996 he moved to Houghten Pharmaceuticals (later renamed Trega Biosciences), the early competitor of Selectide. In 1993, he formed Spyder Instruments, which in 2000 merged with the new startup biotech company Illumina Inc. He has been with Illumina, Inc., San Diego, CA, as Senior Director since then.

Dr. Lebl is the recipient of several awards, the most prestigious being the Leonidas Zervas Award of the European Peptide Society and the 2003 Jouan Award for his contributions to laboratory automation and laboratory process improvement. He is a member of the editorial boards of scientific journals, and serves on the scientific advisory boards of several companies.

Ricardo Gutierrez-Osuna (M'00) received the B.S. degree in electrical engineering from the Polytechnic University of Madrid, Madrid, Spain, in 1992 and the M.S. and Ph.D. degrees in computer engineering from North Carolina State University, Raleigh, in 1995 and 1998, respectively.

From 1998 to 2002, he served on the faculty at Wright State University, Dayton, OH. He is currently an Associate Professor of Computer Engineering at Texas A&M University, College Station. His research interests include pattern recognition, neuromorphic computation, chemical sensor arrays, and audio-visual speech processing.

Dr. Gutierrez-Osuna is a recipient of the National Science Foundation Career Award for his research on machine olfaction with chemical sensors arrays.